Ferredoxin Reduction by Photosystem I from Synechocystis sp. PCC 6803: Toward an Understanding of the Respective Roles of Subunits PsaD and PsaE in Ferredoxin Binding

ARTICLE *in* BIOCHEMISTRY · DECEMBER 1998

Impact Factor: 3.02 · DOI: 10.1021/bi981379t · Source: PubMed

3 AUTHORS, INCLUDING:

Patrick Barth
Baylor College of Medicine
23 PUBLICATIONS **1,264** CITATIONS

SEE PROFILE

Ferredoxin Reduction by Photosystem I from *Synechocystis* sp. PCC 6803: Toward an Understanding of the Respective Roles of Subunits PsaD and PsaE in Ferredoxin Binding

Patrick Barth, Bernard Lagoutte, and Pierre Sétif*

CEA, Département de Biologie Cellulaire et Moléculaire, Section de Bioénergétique, and CNRS URA 2096, C.E. Saclay, 91191 Gif sur Yvette, France

Received June 10, 1998; Revised Manuscript Received August 24, 1998

ABSTRACT: The process of ferredoxin reduction by photosystem I has been extensively investigated by flash-absorption spectroscopy in *psaD* and *psaE* deleted mutants from *Synechocystis* sp. PCC 6803. In both mutants, the dissociation constant for the photosystem I/ferredoxin complex at pH 8 is considerably increased as compared to the wild type: approximately 25- and 100-fold increases are found for PsaD-less and PsaE-less photosystem I, respectively. However, at high ferredoxin concentrations, submicrosecond and microsecond kinetics of electron transfer similar to that observed in the wild type are present in both mutants. The presence of these fast kinetic components indicates that the relative positions of ferredoxin and of the terminal photosystem I acceptor are not significantly disturbed by the absence of either PsaD or PsaE. The second-order rate constant of ferredoxin reduction is lowered 10- and 2-fold for PsaD-less and PsaE-less photosystem I, respectively. Assuming a simple binding equilibrium between photosystem I and ferredoxin, PsaD appears to be important for the guiding of ferredoxin to its binding site (main effect on the association rate) whereas PsaE seems to control the photosystem I/ferredoxin complex lifetime (main effect on the dissociation rate). The properties of electron transfer from photosystem I to ferredoxin were also studied at pH 5.8. In the *psaE* deleted mutant as in the wild type, the change of pH from 8 to 5.8 induces a 10-fold increase in affinity of ferredoxin for photosystem I. In the absence of PsaD, this pH effect is not observed, in favor of this subunit being mostly responsible for the low pH increased affinity.

Photosystem I (PSI)[1] is a light-driven transmembrane oxidoreductase found in oxygenic photosynthetic organisms. Cyanobacterial PSI reaction centers contain at least eleven different polypeptidic subunits (reviewed in ref *1*) and can be isolated in trimeric as well as in monomeric forms (*2*, *3*). Within PSI, the light-induced primary charge separation occurs between the primary donor P700 (a chlorophyll dimer) and the primary acceptor A_0, many other chlorophyll molecules serving as an internal antenna. Charge separation is then stabilized by a fast electron transfer to secondary acceptors which are the phylloquinone A_1 and three different [4Fe−4S] centers named F_X, F_A, and F_B (reviewed in ref *4*). Electron transfer within PSI leads eventually to the formation of $P700^+$ and $(F_A, F_B)^-$. These species are used for oxidation or reduction of soluble proteins located on opposite sides of the photosynthetic membrane. In cyanobacteria, these proteins are respectively cytochrome c_6 or plastocyanin on the lumenal side and ferredoxin (Fd) or flavodoxin on the stromal side. Among the different PSI subunits, the PsaA−PsaB heterodimer constitutes the core of the complex to which are associated different peripheral smaller subunits. Three of them are good candidates for playing a role in the interaction with the soluble acceptors Fd and flavodoxin: PsaC, which binds the terminal electron acceptors F_A and F_B, and PsaD and PsaE which do not carry any cofactor. An X-ray structure at 4.0 Å resolution is available for trimeric PSI from the cyanobacterium *Synechococcus elongatus* (*5*). This structure allowed the researchers to locate most of the antenna chlorophylls and all cofactors except A_1 within the PSI structure. α-helices were also identified, and all of them were tentatively ascribed to given PSI subunits. It is worth noting that the stromal region, which includes subunits PsaC, D, and E, is poorly resolved at the present 4 Å resolution. The approximately 2-fold internal symmetry in PsaC impeded the definite identification of F_A/F_B to the proximal/distal centers. Moreover, it was not possible to fit the known NMR structure of PsaE (*6*) to the electron density in the region presumably occupied by this subunit in the PSI complex (*5*).

The good accessibility of PsaD and PsaE on the stromal side of PSI has been clearly demonstrated in the past (*7*, *8*), and a general spatial organization has been proposed more recently (*5*, *9*). On the basis of cross-linking experiments, the soluble Fd acceptor has been assigned to interact directly with PsaD (*10*, *11*). This last interaction was more precisely characterized by identifying a pair of bridged amino acids between PsaD and Fd in a functional cross-linked complex

* Corresponding author.

[1] Abbreviations: PSI, photosystem I; Fd, ferredoxin; PsaD-, PsaE-, photosystem I prepared from the *psaD* and *psaE* deleted strains, respectively; β-DM, β-dodecyl maltoside; DCPIP, 2,6-dichlorophenol-indophenol; FNR, ferredoxin-$NADP^+$ oxidoreductase; WT, wild type.

10.1021/bi981379t CCC: $15.00
Published on Web 10/30/1998

(*12*). This covalent complex also allowed the localization of Fd by electron microscopy, in close contact with a ridge formed by the subunits PsaC, PsaD, and PsaE (*13*). Despite the supposed close proximity of Fd to PsaE, a cross-linked complex between both proteins has been reported only in barley (*14*). Different approaches favored anyway a role of PsaE in the binding of Fd (*15*, *16*), with a reported 25-fold decrease of the Fd reduction rate when this subunit is absent (*16*). Relatively small effects of *psaE* deletion on the photoautotrophic growth of cyanobacterial strains were reported (*17*, *18*) whereas an involvement of the PsaE subunit in cyclic electron flow has been proposed (*18*, *19*). Concerning PsaD, gene deletion in *Synechocystis* 6803 was first reported to dramatically affect the photoautotrophic growth of the cells (*20*). In such a mutant, the Fd-mediated $NADP^+$ photoreduction was shown to be considerably impaired (*21*, *22*). A direct prominent role of PsaD in the PSI/Fd interactions was also evidenced from the study of deleted and site-directed mutants from *Synechocystis* sp. PCC 6803 (*23*). In the latter study, first-order reduction of Fd was reported to be unobservable in the deleted mutant, and a decrease of at least 10-fold was observed for the second-order process.

With regard to the first report from our laboratory dealing with mutagenesis of PsaE (*16*), experimental conditions for direct detection of Fd reduction were not precisely defined and were reported later (*24*, *25*). Concerning the study of PsaD (*23*), attention was focused onto site-directed mutants, whereas no detailed study of the deleted strain was made with extensive averaging and high Fd concentrations. Therefore it appears that a detailed characterization of Fd reduction by both mutants was still missing. Such data, including characterization of first-order and second-order phases of Fd reduction, are provided by the present study. In turn, obtaining such parameters enables new insights into the respective roles of subunits PsaD and PsaE in the Fd photoreduction process.

EXPERIMENTAL PROCEDURES

Biological Samples. The *psaD* and *psaE* deleted strains of the cyanobacterium *Synechocystis* 6803 were obtained as previously described (refs *23* and *16*, respectively). Thylakoid membranes and *n*-dodecyl β-D-maltoside (β-DM) PSI reaction centers were prepared according to ref *24*, following ref *26* (hereafter designed as PsaD- and PsaE-). Fd from *Synechocystis* 6803 was prepared according to ref *27* with some recent improvements (*28*). Fd overexpressed in *E. coli* was also routinely used (Lagoutte, unpublished data). The kinetics of photoreduction of recombinant Fd by PSI were indistinguishable from that observed with Fd from *Synechocystis*. Membranes from the *psaE* deleted mutant were reconstituted with the isolated PsaE subunit from *Synechocystis* 6803 following the protocol described previously for the reconstitution of the octyl-βD-glucopyranoside purified PSI from the same *psaE* deleted strain (*16*).

Flash-Absorption Spectroscopy. Measurements were made with a square 1 cm cuvette at 296 K as described elsewhere (*24*, *25*). Flash excitation was provided either by a ruby laser (wavelength, 694.3 nm; duration, 6 ns; pulse energy $\approx$ 15 mJ) or by a frequency-doubled YAG laser pumping a dye laser (wavelength, 695 nm; duration, 6 ns; pulse energy $\approx$ 20 mJ). The Fd reduction process was directly put forward by subtracting kinetics observed with PSI alone from that observed in the presence of Fd and by building some composite curves as explained in ref *25*. The subtraction procedure is made necessary by the presence of antenna triplet states decaying in the same time range as that of some components of Fd reduction. Moreover, it allows one to identify the presence of a submicrosecond component of Fd reduction, which is not directly resolved in the present study. Fd reduction by $(F_A, F_B)^-$ can be monitored in the 460−600 nm region (*24*, *25*). In this region, the two wavelengths of 480 and 580 nm are preferentially used because the amplitude of antenna triplets is minimal. Membranes and purified PSI from all mutants were studied at 820 nm for probing the $P700^+$ decay and the possible presence of recombination phases indicative of partial inactivation of electron acceptors. In the case of PsaE-, the decay was comparable to that of the wild type (WT), including less than 5% of a 1 ms component corresponding presumably to a recombination reaction between $P700^+$ and F_X- (*29*). Concerning PsaD-, three fast components were observed besides the slow decay occurring in tens of milliseconds and ascribed to recombination between $P700^+$ and $(F_A, F_B)^-$. These components, accounting for 40% of the total decay at 820 nm, exhibit halftimes of 5 μs, 100 μs, and 1 ms and are ascribed to recombination reactions between $P700^+$ and A_1^- or F_X^- in partially degraded PSI (*29*−*31*). The concentration of PSI reaction centers was calculated from photoinduced absorption changes at 820 nm, assuming an absorption coefficient of 6500 M^{-1} cm^{-1} for $P700^+$ (*32*). Measurements were also made with a 1 × 0.2 cm^2 cuvette: the cuvette face was placed almost perpendicular to the measuring beam (angle between the cuvette face and the beam < 15°) so that the optical path is very close to 0.2 cm (between 0.2 and a maximum value of 0.204 cm when taking into account the refractive index of glass and water); the exciting light beam was perpendicular to the cuvette face; the smaller volume and light path of such cuvettes allowed the use of higher Fd concentrations (up to 90 μM).

Determination of the Dissociation Constants K_d. For both *psaD* and *psaE* deleted mutants, dissociation constants corresponding to the PSI−Fd complex were estimated at pH 8.0 from the dependence of the fast signal of Fd reduction at 580 nm upon Fd concentration. Estimation of this fast signal was made for each Fd concentration in several steps: First, the composite curve directly exhibiting Fd reduction was obtained (see above). Second, the characteristics (rate and amplitude) of the slowest phase were obtained by fitting the absorption change with a single exponential component without taking into account the initial fast decay (presumably due to first-order components); the rate of this slow process depends on the Fd concentration (linear dependence up to $\approx$16 μM), showing that it can be ascribed to diffusion-limited second-order Fd reduction (at least up to [Fd] = 16 μM). Third, this slowest phase is extrapolated to zero time: the initial absorption change thus obtained is ascribed to faster first-order components. Characterization of the faster components leading to their identification as first-order phases of Fd reduction is described in the Results section. For both mutants, the total amplitude of first-order components was plotted versus Fd concentration, and these data were fitted assuming a simple binding equilibrium between PSI and Fd.

The maximum size of this amplitude is obtained from the sum of amplitudes of all phases of Fd reduction (first- + second-order components) and is used as a fixed parameter during the fits. For the *psaE* deleted mutant, K_d at pH 5.8 was obtained similarly using Fd concentrations up to 8 μM.

Chemical Cross-Linking of PsaE- and Fd. A protocol similar to that previously described (*12*) was used, with modified concentrations of PSI and Fd to partly overcome the effects of the decreased affinity. Final concentrations of PSI and Fd were, respectively, 0.5 μM and 10 μM, in MES buffer pH 7.0, 50 mM, β-DM 0.03%. The two chemical reagents, EDC (1-ethyl-3-(3-dimethylaminopropyl)-carbodimide from Sigma) and NHS (*N*-hydroxysulfosuccinimide from Fluka), were added together at a final concentration of 2 mM. $MgCl_2$ was increased to a final concentration of 20 mM, and the reaction proceeded at 25 °C during 1 h. The sample was then directly washed/concentrated using a centriprep 100 (Amicon). Transient signals of a PSI preparation to which Fd has been cross-linked and of a control sample pretreated with the chemical cross-linker in the absence of Fd were recorded in the 460−600 nm region. The subtracting procedure described above was used in order to put forward directly the kinetics of Fd reduction and was performed after precisely adjusting the concentrations of the two samples for a proper comparison.

Electron Paramagnetic Resonance Spin Quantification. Electron paramagnetic resonance (EPR) spin quantification was performed by two methods: (a) the relative stoichiometries of ferredoxin and (F_A, F_B) clusters were determined as described in ref *12* in a PSI−Fd cross-linked sample prepared from the *psaE* deleted mutant. Spin amounts in the control and cross-linked samples were compared under reducing conditions allowing full reduction of F_A, F_B, and Fd with minimal amounts of reduced F_X. (b) Relative stoichiometries of $P700^+$ and Fd were obtained in the following way: a reference sample was prepared containing reduced Fd at a known concentration. It was compared to a reduced cross-linked sample by EPR at 50 K under nonsaturating conditions. At this temperature, only ferredoxin is observable, allowing the direct quantification of the content of Fd in the cross-linked sample. The PSI concentration in the cross-linked sample was derived from flash-absorption measurements at 820 nm at room temperature (see above). Both methods give comparable results, but the second procedure was found to be more precise, especially when the amount of cross-linked Fd is relatively low (<1 per PSI).

RESULTS

Fd Reduction by PsaE- at pH 8. Fd reduction by PsaE- was studied at pH 8 in the presence of salts (30 mM NaCl, 5 mM $MgCl_2$); these conditions are identical to those previously used for the detailed characterization of WT PSI (*24*, *25*). Figures 1 and 2 show the kinetics of Fd reduction (see Experimental Procedures) on time scales of 10 ms and 400 μs, respectively. For Fd concentrations below 16 μM, a major phase of Fd reduction was observed between 460 and 600 nm on a millisecond time scale. The signal recorded at 480 nm is shown for three different Fd concentrations (Figure 1, part A). The rate of this phase exhibits a linear dependency upon Fd concentration ([Fd] ≤ 16 μM; part B).

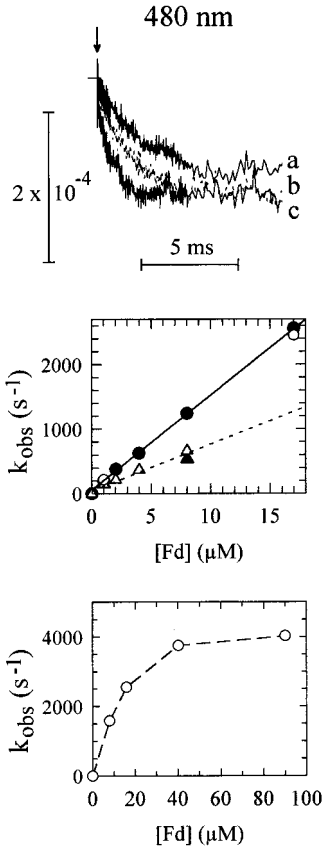

FIGURE 1: Reduction of Fd by PSI and membranes prepared from the *psaE* deleted mutant. Part A: kinetic traces at 480 nm of Fd reduction by PSI monomers (≈0.25 μM) at different Fd concentrations (a, 2.02 μM; b (dotted line), 4.0 μM; c, 8.0 μM) (480 nm, 10 ms time scale). Parts B and C: rate of the slower reduction phase as a function of Fd concentration. Rates were measured at 480 nm (closed symbols) and 580 nm (opens symbols) for either PSI (circles) or membranes (triangles). Linear fits (part B) correspond to second-order rate constants of 1.47×10^8 M^{-1} s^{-1} (continuous line) and 0.72×10^8 M^{-1} s^{-1} (dotted line) for PSI and membranes, respectively. All measurements were made in 20 mM Tricine, pH 8, in the presence of 0.03% β-DM, 30 mM NaCl, 5 mM $MgCl_2$, 1.5 mM sodium ascorbate, and 30/40 μM 2,6-dichlorophenolindophenol (DCPIP). Averages of 32−96 experiments were recorded both in the presence and absence of Fd. Repetition rate of laser flash excitation: 0.1 Hz. Parts A and B: optical path, 1 cm; [PSI] ≈ 0.25 μM. Part C: optical path, 0.2 cm; [PSI] ≈ 1.28 μM.

Under identical conditions of Fd concentration, salts, and pH, the rate observed with isolated PSI is about twice larger than that with membranes. Second-order rate constants of 1.5×10^8 M^{-1} s^{-1} and 0.7×10^8 M^{-1} s^{-1} can be derived for Fd reduction by PSI and membranes, respectively. The 2-fold decrease observed with the membranes versus PSI may arise from electrostatic repulsion due to negative charges carried by the membrane lipids. By comparison to these values, a second-order rate constant of $(2-5) \times 10^8$ M^{-1} s^{-1} has been estimated for WT PSI (*24*; the rate was not measured for the WT membranes). The large contribution of the second-order process with PsaE- allowed a precise determination of its rate constant. This is not the case for WT PSI, Fd reduction being mostly a first-order process when studied under conditions appropriate for getting a reasonable signal-to-noise ratio in flash-absorption experiments, i.e., in the micromolar range. In addition, WT kinetics are complicated by not fully understood absorption changes occurring in the same time range as the second-order process

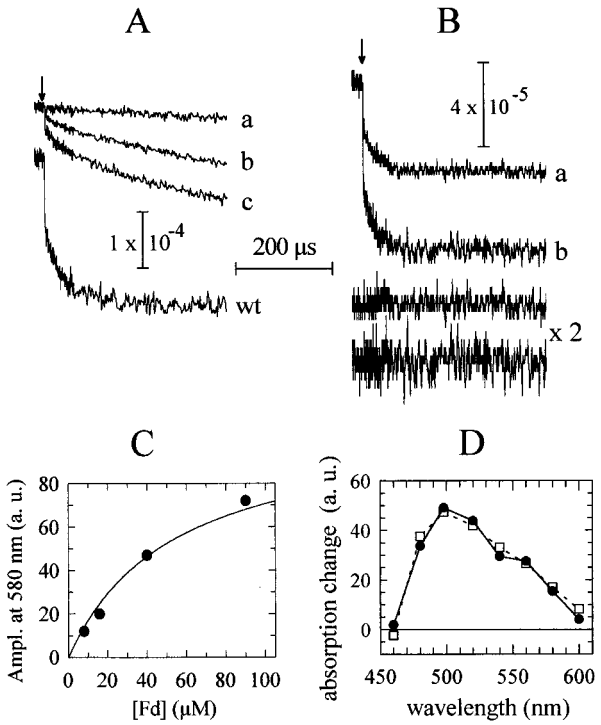

FIGURE 2: First-order reduction of Fd by PSI prepared from the *psaE* deleted mutant. The measurements were performed under conditions similar to those for Figure 1. Part A: kinetic traces of Fd reduction at 580 nm at different Fd concentrations (a, 1.01 μM; b, 8.1 μM; c, 17.0 μM). A control experiment with WT PSI (wt, 0.255 μM) is also shown ([Fd] = 2.17 μM). Part B: kinetic traces at 580 (trace a) and 480 nm (trace b) exhibiting Fd reduction ([Fd] = 14.4 μM; [PSI] = 0.25 μM), after subtraction of the second-order decay. The two traces were fitted by a biexponential decay using a global fit procedure, resulting in $t_{1/2}$ of 16 and 377 μs ascribed to first- and second-order phases, respectively. The 377 μs phase was subtracted from the experimental decay in order to put forward the first-order phases (unresolved submicrosecond component and 16 μs phase; see text). Residuals (multiplied by 2) are shown below the experimental curves. Part C: sum of amplitudes (in arbitrary units) of fast phases at 580 nm obtained by extrapolating the slowest phase to zero time (see Experimental Procedures). The continuous line corresponds to a fit assuming a simple binding equilibrium between PSI and Fd (the maximum size of the signal is used as a fixed parameter; see Experimental Procedures); it corresponds to K_d = 52 μM. Part D: spectrum of the first-order phases of Fd reduction ([Fd] = 15.5 μM; [PSI] = 0.27 μM). The spectrum (closed circles) was obtained by measuring the signal decrease 40 μs after the flash. The contribution of the second-order process was subtracted from such signals. For comparison, the calculated spectrum for electron transfer from $(F_A, F_B)^-$ to Fd is shown after normalizing the areas under the spectra between 460 and 600 nm (open squares). Parts A, B, and D: optical path, 1 cm; [PSI] $\approx$ 0.25−0.27 μM. Part C: optical path, 0.2 cm; [PSI] $\approx$ 1.28 μM.

(*25*). Fd reduction was also studied at higher concentrations in a flat cuvette (see Experimental Procedures, part C of Figure 1): the rate of the slowest phase appears to deviate from a linear dependence, reaching an asymptotic value of $\geq$4000 s^{-1}. This may be related to some limiting step of Fd reduction. Note, however, that the contribution of the slowest phase becomes minor at the highest Fd concentration (90 μM) so that the rate determination becomes less precise than that at lower Fd concentrations.

On a shorter time scale, the kinetics recorded at 580 nm (Figure 2, part A) show faster components preceding the second-order decay. Traces a, b, and c were obtained with Fd concentrations of 1, 8, and 17 μM, respectively, and can be compared with the trace of a WT PSI (trace wt) (2.2 μM of Fd). The fast components recorded on this time scale and ascribed to first-order processes are much smaller with PsaE- than with WT PSI. These first-order components are better seen after subtraction of the second-order decay contribution. The resulting kinetics are shown in part B of Figure 2 (trace a, 580 nm; trace b, 480 nm). A fast unresolved phase ($t_{1/2}$ < 1 μs) is clearly present together with an absorption decrease in the microsecond range. At both wavelengths, the kinetic analysis shows that the microsecond decay can be fitted with a single component with $t_{1/2} \approx 16$ μs (see residuals in part B). The same kinetic pattern of fast components is observed at higher Fd concentrations (up to 90 μM) after subtraction of the slower component, in line with the assignment of these components to first-order phases. In previous studies, the presence of three different first-order phases of Fd reduction by WT PSI from *Synechocystis* has been reported, with $t_{1/2} \approx$ 500 ns, 15 μs, and 100 μs (*24*, *25*). The kinetics of Fd reduction by PsaE- can be described with only two components (<1 and $\approx$16 μs). The spectrum of these fast components is shown in part D of Figure 2, by plotting the signal at 40 μs after the flash between 460 and 600 nm, after corrections for the second-order process (closed circles, [Fd] = 15.5 μM). The shape of this spectrum is almost indistinguishable from the spectrum which can be calculated for reduction of Fd by $(F_A, F_B)^-$ (open squares) (*25*). Thus the present data indicate clearly that PsaE- and Fd can form a complex undergoing fast (submicrosecond and microsecond) reduction of Fd. This precise kinetic study was performed after extensive averaging using 1 cm cuvettes. On a later stage, experiments with flat cuvettes allowing the use of higher Fd concentrations were performed for measuring the total amount of first-order components as a function of Fd concentration (see Experimental Procedures). This is shown in part C of Figure 2: assuming a simple binding equilibrium, a dissociation constant of 52 μM was calculated (continuous curve), corresponding to approximately a 100-fold decrease in affinity compared to WT ($\approx$0.5 μM; (*24*, *25*)).

Control Studies: Reconstitution and Chemical Cross-Linking Experiments. A PsaE deleted strain sample was reconstituted with the homologous PsaE subunit purified from WT membranes of *Synechocystis* 6803 as previously described (*16*). After such a reconstitution, PSI recovered the ability to rapidly reduce Fd at micromolar concentrations of Fd. This is shown in part A of Figure 3 for Fd concentrations of 0.8 and 3.3 μM. A submicrosecond decay followed by at least a component in the microsecond time range is visible. Fast kinetics were recorded under identical conditions for a series of increasing Fd concentrations. The amplitudes of the signals at 300 μs after the flash have been plotted versus the Fd concentration (part B of Figure 3). These data were fitted assuming a simple binding equilibrium between PSI and Fd. A value of 1.06 μM is found for the dissociation constant, which is only twice larger than the WT value ($K_d \approx$ 0.5 μM; (*24*, *25*)). The asymptotic value of the fit corresponds to 75% of the value that is observed with WT PSI or membranes. The presence of a second-order phase of Fd reduction accounts for the missing part of the signal. These data indicate that about 75% of PSI have been functionally reconstituted with PsaE.

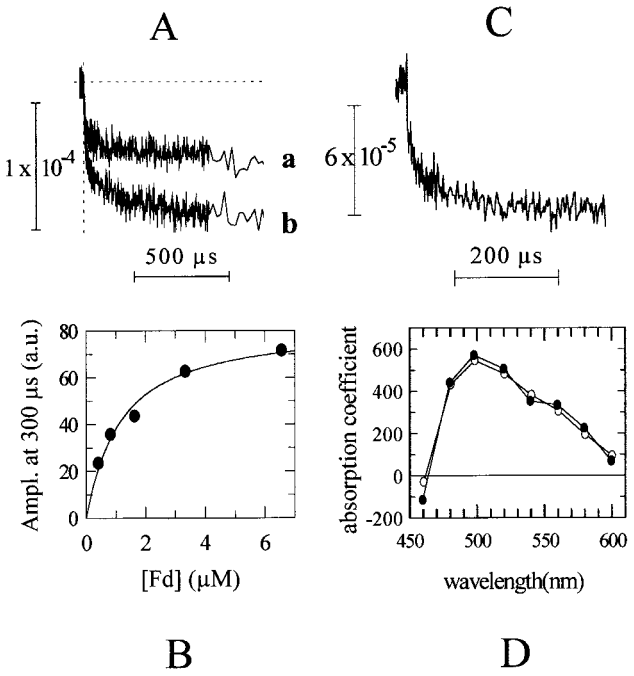

FIGURE 3: Reduction of Fd in a PsaE reconstituted sample (left part) and in PsaE-/Fd covalent complexes (right part). Part A: kinetic traces of Fd reduction at 580 nm at two different Fd concentrations—0.81 μM (a) and 3.33 μM (b) ([PSI] = 0.17 μM). Part B: absorption changes measured 300 μs after the flash as a function of the Fd concentration. The absolute values of the negative signals are plotted in arbitrary units. The curve corresponds to data fitting, assuming a simple binding equilibrium between PSI and Fd. The dissociation constant K_d and the maximum amplitude A_{max} were adjustable parameters: $K_d = 1.06$ μM and $A_{max} = 82$. This last value corresponds to $\Delta A = 1.15 \times 10^{-4}$ which represents 75% of the maximum signal observed with WT membranes. All measurements were made in 20 mM Tricine, pH 8, in the presence of 0.03% β-DM, 30 mM NaCl, 5 mM $MgCl_2$, 1.5 mM sodium ascorbate, and 30 μM DCPIP, in square 1 cm cuvettes. Averages of 64 experiments were recorded both in the presence and absence of Fd. Part C: kinetic trace at 580 nm of Fd reduction in PsaE-/Fd cross-linked complexes. The measurements were performed under conditions similar to those for Figure 1, except [DCPIP] = 15 μM, averages were of 16 experiments, and [PSI] = 0.269 μM. Part D: Decay-associated spectrum due to Fd reduction in the covalent PSI−Fd complex (closed circles), as obtained by measuring the signal decrease 200 μs after the flash. For comparison, the calculated spectrum for electron transfer from $(F_A, F_B)^-$ to Fd is shown after normalizing the areas under the spectra between 460 and 600 nm (open squares).

A previous study allowed the isolation of a functional, one to one, chemically cross-linked complex between PSI and Fd (*12*). A major cross-linked product was obtained between Fd and PsaD, with an almost complete disappearance of free PsaD. We repeated the same type of experiment with PsaE-, using somewhat different conditions to compensate for the decreased Fd affinity (see Experimental Procedures). The reduction of Fd in this cross-linked complex was analyzed by laser flash-absorption spectroscopy (part C of Figure 3, see Experimental Procedures). Submicrosecond and microsecond components similar to those observed in the noncovalent complex are still present. A plot of the absorption decay between 460 and 600 nm at 200 μs after the flash (part D of Figure 3, closed circles) shows the spectrum of the fast components, fitting almost exactly the calculated spectrum for reduction of Fd by $(F_A, F_B)^-$ (open circles). Thus, these results show unambiguously that the observed fast kinetics corresponds to the reduction of the Fd cross-linked to the PsaE deleted PSI in a position similar to that in the noncovalent WT complex. For spectral comparison, the calculated spectrum was multiplied by a factor of 0.21, indicating that fast reduction of Fd occurs in ≈21% of the PSI reaction centers. An EPR spin quantification performed at 25 K under nonsaturating conditions indicates the presence of 0.66 Fd per PSI reaction center in the covalent complex (see Experimental Procedures). One-third of Fd thus appears to be functionally cross-linked, which is twice lower than the values obtained with WT PSI (*13*). Considering the low affinity of Fd for the PsaE- ($K_d \approx 50$ μM), competition between physiological and nonspecific binding sites in this irreversible reaction may become critical, accounting for the decreased proportion of Fd correctly cross-linked to PSI.

Fd Reduction by PsaE- at pH 5.8. When studied at pH 5.8 in the absence of salts, the affinity of Fd for WT PSI was found to be about 10-fold higher than that at pH 8 in the presence of salts ($K_d \approx 0.05$ μM versus 0.5 μM) (*25*). We also studied reduction of Fd by PsaE- at acidic pH in order to examine the possible contribution of PsaE to this pH dependence (Figure 4). The kinetics of this process were recorded for a series of increasing Fd concentrations. As can be seen from the residuals of the fits performed on such a signal at 580 nm (Figure 4, part A, [Fd] = 8 μM), two exponential components in the microsecond−millisecond time range are necessary to describe satisfactorily the kinetics of Fd reduction. The dependence of these components upon Fd concentration shows that the fastest one is first-order ($t_{1/2} \approx 10$ μs) and the slowest one is second-order. A third submicrosecond component, which is not resolved in the present study and is also first-order, is clearly visible on a 400 μs time scale and corresponds to the initial amplitude in the fit of Figure 4. Compared to the same process already described at pH 8 (Figures 1 and 2), the first-order phases are much larger. Their kinetic pattern is similar to that of WT PSI at pH 5.8 with the presence of both one submicrosecond component and one microsecond component of 10 μs halftime. The slowest component of Fd reduction can be observed on a longer time scale (data not shown). Its rate depends linearly upon Fd concentration (Figure 4, part C) with a second-order rate constant of 4.7×10^8 M^{-1} s^{-1}. This rate constant is 3 times larger than that measured at pH 8 with salts. Such a rate constant could not be measured for WT, due to the high Fd affinity. The sum of amplitudes due to submicrosecond and 10 μs components was plotted versus the Fd concentration (Figure 4, part B). These data were fitted assuming a simple binding equilibrium between PSI and Fd, and a value of 3.4 μM was found for the dissociation constant. Therefore, a pH shift from 8.0 to 5.8 induces an affinity increase of the same order (≈15-fold increase) as for WT PSI (≈10-fold increase).

Fd Reduction by PsaD-. Figure 5 shows the kinetics of Fd reduction by PsaD- on time scales of 400 μs (part A) and 10 ms (part D). On the longer time scale, a large phase of Fd reduction can be observed. Its rate exhibits a linear dependency upon Fd concentration (part E), and a second-order rate constant of $(2.7 \pm 0.5) \times 10^7$ M^{-1} s^{-1} can be derived from a linear fit of the data. This rate constant is about 10 times smaller than that of WT PSI. It can be noted that, contrary to the case of PsaE-, the amplitude of the

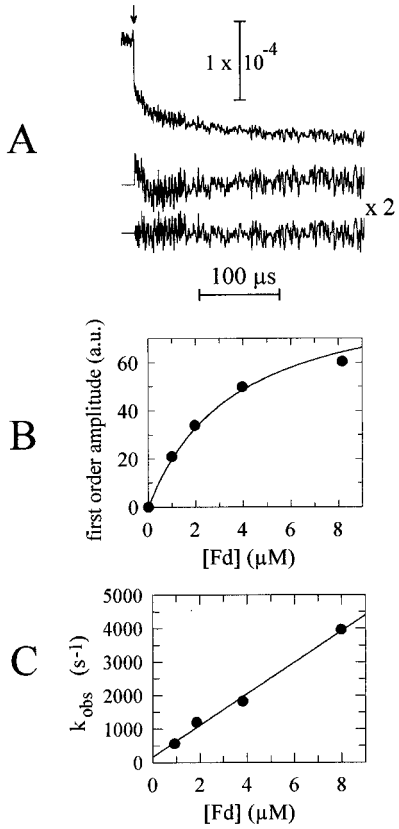

FIGURE 4: Reduction of Fd by PsaE- at pH 5.8 in the absence of salts. Part A: kinetics of Fd reduction at 580 nm with PsaE- and Fd concentrations of 0.23 and 8.2 μM, respectively. Measurements were performed in square 1 cm cuvettes under the following conditions: repetition rate, 0.1 Hz; 2 mM sodium ascorbate; 250 μM DCPIP; averages of 32 experiments. Residuals (multiplied by 2) are shown below. The upper residuals correspond to a monoexponential fit: initial amplitude (unresolved submicrosecond component), 0.75×10^{-4}; $t_{1/2} = 66$ μs, 0.53×10^{-4}; offset (longer-lived absorption change), 1.28×10^{-4}. The lower residuals correspond to a biexponential fit: initial amplitude, 0.56×10^{-4}; $t_{1/2} = 9.9$ μs, 0.38×10^{-4}; $t_{1/2} = 172$ μs, 0.38×10^{-4}; offset, 1.33×10^{-4}. Part B: the sum of amplitudes of the submicrosecond component and the 10 μs components was plotted versus Fd concentration. Assuming a simple binding equilibrium, a dissociation of 3.4 μM was calculated. Part C: the rate of the slower component was plotted versus Fd concentration. A linear fit is shown giving a second-order rate constant of 4.7×10^8 M^{-1} s^{-1}.

second-order component is so small at high Fd concentrations that determination of its rate cannot be performed for [Fd] > 20 μM. On a shorter time scale (part A), some fast components preceding the second-order decay are also present. A submicrosecond component is clearly visible whereas a minor microsecond component most probably precedes the second-order phase. However, the small amplitude of this component did not allow a reliable determination of its halftime. The general shape of the spectrum due to the fast components (part C) clearly indicates that these phases correspond to electron transfer from $(F_A, F_B)^-$ to Fd. In part B, the amplitude of the fast components is plotted versus Fd concentrations up to 90 μM (2 mm of optical path): assuming a simple binding equilibrium, a dissociation constant of 13 μM was calculated (continuous curve), corresponding to approximately a 25-fold decrease in affinity compared to WT. Such first-order components were not observed in a previous study (*23*) for reasons which are not fully understood. The present observations were

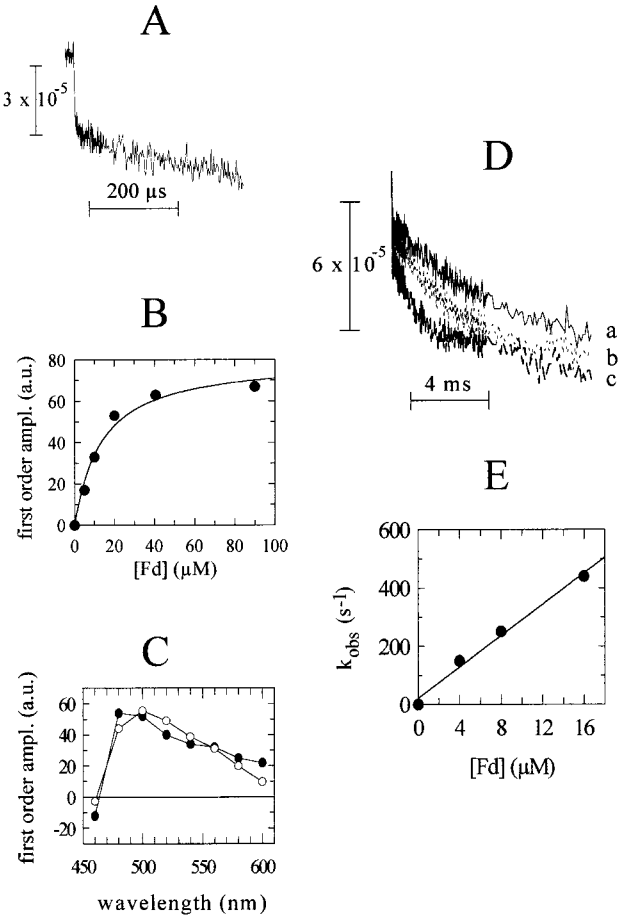

FIGURE 5: Reduction of Fd by PsaD-. Part A: kinetic trace of Fd reduction at 580 nm ([PSI] = 0.100 μM; [Fd] = 16 μM). The measurements were performed under conditions similar to those of Figure 1, except the averages were of 128 experiments. Part B: sum of amplitudes (in arbitrary units) of fast phases at 580 nm obtained by extrapolating the slowest phase to zero time (see Experimental Procedures). The continuous line corresponds to a fit assuming a simple binding equilibrium between PSI and Fd (the maximum size of the signal is used as a fixed parameter; see Experimental Procedures); it corresponds to $K_d = 12.8$ μM. Part C: spectrum of first-order phases of Fd reduction ([Fd] = 16 μM; [PSI] = 0.137 μM), obtained by measuring the signal decrease 200 μs after the flash (closed circles). For comparison, the calculated spectrum for electron transfer from $(F_A, F_B)^-$ to Fd is shown after normalizing the areas under the spectra between 460 and 600 nm (open squares). Part D: kinetic traces of Fd reduction ([PSI] = 0.137 μM) at different Fd concentrations (a, 4.0 μM; b (dotted line), 8.0 μM; c, 16.0 μM) (580 nm, 10 ms time scale). Part E: slower phase of Fd reduction recorded at 580 nm as a function of Fd concentration. A linear fit is shown, giving a second-order rate constant of $(2.7 \pm 0.5) \times 10^7$ M^{-1} s^{-1}.

made after extensive averaging and with high Fd concentrations, which has allowed the unambiguous detection of the presence of these phases. These new results demonstrate that even in the absence of PsaD, PSI and Fd can still form a complex undergoing fast reduction of Fd.

In parallel to the study of PsaE-, Fd reduction by PsaD- was also studied at pH 5.8 in the absence of salts. On a short time scale, no fast kinetics of Fd reduction was observed under the range of Fd concentrations used (up to 16 μM). From the absence of such signals, a lower limit of 100 μM was estimated for K_d of Fd with PsaD-. Nevertheless, a slow phase of Fd reduction was still observed on a millisecond time scale (not shown), and the second-order

Table 1: Parameters of Fd Reduction by WT PSI, PsaD-, and PsaE-[a]

	pH 8 with salts (30 mM NaCl, 5 mM $MgCl_2$)						pH 5.8 without salts			
	K_d (μM)	/WT[a]	k'_{on} (10^8 M^{-1} s^{-1})	/WT[a]	k_{off} /WT[a]	characteristics of first-order kinetics	K_d (μM)	/WT[a]	k'_{on} (10^8 M^{-1} s^{-1})	characteristics of first-order kinetics
WT	0.5	1	3.5 ± 1.5	1	1	3 phases: <1, 10, 100 μs	0.05	1	n.o.	2 phases: <1, 10 μs
PsaD-	13	25	0.27	≈0.1	2.5[b]	2 phases: <1 μs, *c*	>100	>2000	0.07/0.2	n.o.
PsaE-	52	100	1.5	≈0.5	50[b]	2 phases: <1, 16 μs	3.4	70	4.7	2 phases: <1, 10 μs

[a] Ratios between values of mutant and WT. [b] Only ratios with a WT value have been calculated (see text). [c] Minor microsecond component, $t_{1/2}$ not determined; n.o. = not observed.

Scheme 1

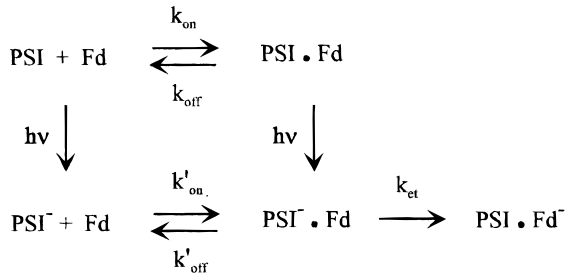

rate constant of this process was found to lie between 0.7 and 2.0×10^7 M^{-1} s^{-1}.

DISCUSSION

Purified PSI from *Synechocystis* 6803 isolated either from PsaD or PsaE deleted strains were already used for in vitro studies of Fd reduction. In a first report on PsaE-, Fd reduction could not be directly detected and its rate was estimated from indirect measurements of $P700^+$ decay (*16*). Similar indirect measurements were more recently reported for PsaD-, though in that case, it was possible to directly observe a slow second-order Fd reduction process ($k < 0.5 \times 10^8$ M^{-1} s^{-1}; (*23*)). It was found that, in both cases, the rates of Fd reduction were considerably decreased when compared to the WT whereas no first-order component indicative of Fd reduction within a preformed PSI/Fd complex was reported. The present work allows a precise measurement of kinetic parameters with both deleted mutants which are given in Table 1 and can be interpreted within Scheme 1, where PSI^- stands for PSI with an electron on (F_A, F_B) and where (PSI·Fd) stands for a complex competent for fast electron transfer. The upper equilibrium is established in darkness, whereas the lower part of the scheme corresponds to reactions occurring after the flash excitation. In kinetics directly exhibiting Fd reduction, the amount of first-order phases is ascribed to PSI·Fd complexes which are formed before flash excitation. From the dependence of this amount versus Fd concentration, the dissociation constant in darkness $K_d = k_{off}/k_{on}$ has been evaluated for WT and deleted PSIs. The observed second-order process of Fd reduction involves PSI without bound Fd before flash excitation and thus allows the measurement of the rate k'_{on}, under conditions where formation of (PSI^-·Fd) is rate-limiting (linear dependence of k_{obs}).

As noted above, for both deleted mutants, there was no reported evidence for a first-order process of Fd reduction. The new improved data presented in this work show the formation of such complexes and allow the calculation of dissociation constants. The measured K_ds for the PsaD and PsaE deleted mutants were, respectively, 25- and 100-fold larger than that for WT (Table 1). From the present results, the high affinity of Fd for WT PSI ($K_d \approx 0.5$ μM) thus clearly depends on the presence of both PsaD and PsaE subunits. The second-order rate constant of Fd reduction k'_{on} is only reduced about twice in the PsaE- mutant whereas the rate of the same process in the PsaD- mutant is reduced approximately 10-fold. This indicates that the overall electrostatic guiding (*33*−*35*) allowing Fd to reach its docking site is weakly affected by the absence of PsaE (similar k'_{on}) but more severely modified by the absence of PsaD.

With $k_{off} = K_d k_{on}$, the relative effect of a mutation on the k_{off} rate is given by the following equation:

$$k_{off}(\text{Mut})/k_{off}(\text{WT}) = [k_{on}(\text{Mut})/k_{on}(\text{WT})][K_d(\text{Mut})/K_d(\text{WT})]$$

If the presence of an electron on (F_A, F_B) changes to some extent the k_{on} rate, we will assume this change to be of the same order in WT and mutated PSI. The following equation accounts for this last assumption:

$$k'_{on}(\text{Mut})/k'_{on}(\text{WT}) = k_{on}(\text{Mut})/k_{on}(\text{WT})$$

Within this assumption, the dissociation rate constants k_{off} can then be determined from comparisons of K_d and k'_{on}, and the main effect of PsaE absence thus appears to be a 50-fold increase of the k_{off} rate, whereas the effect of PsaD absence on this rate is limited to a 2.5-fold increase.

In PsaE-, the kinetics of electron transfer within the preformed complex exhibits submicrosecond and microsecond components. The first-order kinetic pattern is similar to WT at pH 5.8, whereas at pH 8.0, the slowest component ($t_{1/2} \approx 100$ μs) observed in WT PSI seems absent in PsaE-. The origin of the kinetic complexity observed in WT is still unknown but it can be considered that fairly similar first-order kinetics are observed in WT PSI and PsaE-. Considering that the kinetics of electron transfer is strongly dependent upon the relative distance and orientation of the reaction partners (*36*, *37*), this implies that the geometry of the PSI/Fd complex is not greatly disturbed by the absence of PsaE. Consequently, the structures of the other stromal subunits likely involved in Fd binding, mainly PsaC and PsaD, should not be largely modified by the absence of PsaE. The likely absence of indirect structural effects on PsaD is in line with the present view of the cyanobacterial PSI stromal side, in which subunits PsaD and PsaE make little contacts (*5*, *9*), though some partial overlapping between these two subunits has been claimed (*21*, *38*). The recovery of the WT behavior upon reconstitution of PsaE- with isolated PsaE (75% recovery of fast Fd reduction), as well as the isolation of a

functional covalent complex Fd/PsaE- which undergoes fast Fd reduction, also argues against indirect structural effects.

PsaD has been reported to have a general role in the stabilization of PsaC (*22*, *39*). A recent report on a PsaD-deleted strain (same as used in the present study) showed that both PsaC and PsaE are still present in the PSI complex (*9*, *23*). Reconstitution experiments also clearly demonstrated that a major fraction of these two subunits is still functionally associated to PsaD- (80% recovery of fast Fd reduction; (*23*)). In this last study, it was reported that *psaD* deletion results in a minor modification of the EPR spectra of (F_A, F_B) centers with preferential photoreduction of F_B at low temperature. A similar observation has been also reported by other groups (*22*, *39*). In contrast to this minor effect, a prominent role of PsaD in the PSI/Fd interactions was evidenced from the study of site-directed and deleted mutants (*22*, *23*). In the present study, it was found that the absence of PsaD does not impede the formation of a PSI/Fd complex undergoing fast reduction of Fd. The fast kinetics observed within the PsaD-/Fd complex can be assigned to reduction of Fd by the $(F_A, F_B)^-$ centers. Minor deviations in the spectra of the fast phases compared to the WT spectra were observed which could arise either from little changes in the geometry of the PSI/Fd complex or from small effects on the $(F_A, F_B)^-$ centers. These results argue for the contribution of another polypeptide, besides PsaD and PsaE, in binding Fd in a favorable position for fast electron transfer. An evident candidate for this role is PsaC, which is supported by a recent work made with the green alga *Chlamydomonas reinhardtii* showing that residue K35 of PsaC is a main interaction residue between PsaC and Fd (*40*). Finally, all these data lead us to propose that the binding site for Fd could be shared between PsaC, PsaD, and PsaE with several interaction sites distributed along the stromal ridge formed by these three subunits. It is also quite possible that stromal exposed parts of PsaA/B are involved in Fd binding. Within these assumptions, even in the absence of either PsaD or PsaE, Fd could still find a minimum set of interacting residues for a functional association to PSI.

From studies made on *psaD* site-directed mutants in the region of the Fd cross-linking site (*23*), the unique histidine of PsaD (His 97) was found to contribute largely to the increased affinity of Fd for PSI at low pH. In the present study, an increase of Fd affinity for PsaE- at acidic pH was observed of approximately the same magnitude as for WT PSI. This is a strong indication that PsaE is not involved in this pH effect and supports the view that PsaD plays a prominent role in the pH control of Fd affinity observed in WT PSI as well as in PsaE-. Apart from His 97, other residues of PsaD may take part in this effect. In contrast to the observations made on PsaE-, the affinity of Fd for PsaD- at low pH is decreased by a factor of at least 10 (K_d > 100 μM) compared to that at pH 8.0. This loss of affinity has not been explained for the moment but could arise from regions on the PSI stromal side no longer shielded by PsaD and becoming disruptive for the PSI/Fd complex at this lower pH.

The present results allow us to propose a tentative description of the respective roles of PsaD and PsaE subunits in the Fd photoreduction process.

(i) Both subunits are responsible for the final high affinity of PSI for Fd but for different reasons: whereas PsaE seems to control the lifetime of the PSI/Fd complex, PsaD appears to be important for the electrostatic guiding of Fd to its binding site. The different effects on K_d, k_{on}, and k_{off} are schematically illustrated in Figure 6.

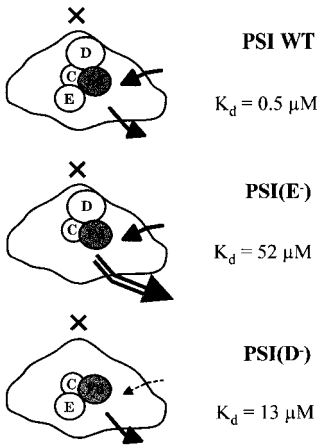

FIGURE 6: Schematic view of parameters governing the binding equilibrium between Fd and WT PSI, PsaE-, and PsaD-. PSI is viewed perpendicularly to the membrane plane with X indicating approximately the trimer symmetry axis. In each case, the upper and lower arrows represent association and dissociation rates, respectively. The width of the arrows corresponds qualitatively to the relative values of the rates (see Table 1).

(ii) PsaD appears to be the main subunit responsible for the pH effect observed with WT PSI.

(iii) In the absence of either PsaD or PsaE, many properties are conserved compared to WT, despite the important loss of affinity (fast kinetics, structure of the remaining stromal subunits).

(iv) PsaC (*40*), and maybe other parts of the PSI core heterodimer, play a role in controlling the geometry of the PSI/Fd complex required for fast electron transfer. Our data support the existence of an extended binding site for Fd, mostly shared between PsaC, PsaD, and PsaE.

This model assumes that, in PsaD or PsaE deleted PSI, unmasking of residues (e.g., stromal loops of PsaA/PsaB) which are normally buried within the complex or other structural effects on the remaining subunits do not lead to large effects on the Fd reduction process which could dominate over direct effects of subunit deletion. Quite evidently, such a possibility cannot be disregarded and, for example, could explain pH effects on PsaD-. However, evidence for complex formation and fast first-order kinetics with both deleted mutants argue against major structural perturbations within the PSI/Fd complexes. This does not exclude indirect effects on association rates (k'_{on}) though the parallel behavior in pH dependence in WT and PsaE- PSI can be taken as an evidence against such indirect effects in the case of subunit PsaE. The model needs to be tested further with site-directed mutants of both *psaD* and *psaE* genes. The present study shows the usefulness of determining together dissociation constants and association constants with high precision in order to assess precisely the possible role(s) of a given residue.

In barley, PsaE has been shown by cross-linking experiments to lie in close proximity to ferredoxin-$NADP^+$ oxidoreductase (FNR) (*41*). In the case of the cyanobacterium *Synechococcus* sp. PCC 7002, it has been shown that FNR contains a N-terminal extension compared to chloro-

plastic enzyme (*42*). This extension is similar to a structural component of phycobilisomes, and a hypothetic model has been proposed recently for the association of phycobilisomes with PSI, which allows FNR to be located very close to the PSI stromal subunits, especially PsaE (*43*). The present results indicate that PsaE could serve to extend the duration of the PSI/Fd complex. It can be speculated that this could be important for Fd to interact with a closely associated FNR, whether FNR is bound to PsaE or indirectly associated to PSI, as may be the case in chloroplast and cyanobacteria, respectively. In turn, this could explain the involvement of PsaE in cyclic electron transport, if such an electron pathway involves FNR being closely associated with PSI. In the absence of PsaE, Fd would dissociate from PSI much more rapidly, thus decreasing the probability of transferring its electron to a nearby partner.

ACKNOWLEDGMENT

We are especially grateful to Dr. H. Bottin for providing upper grade Fd from *Synechocystis* 6803 and for discussions.

REFERENCES

1. Golbeck, J. H. (1994) in *The Molecular Biology of Cyanobacteria* (Bryant, D. A., Ed.) pp 319−360, Kluwer Acad. Publ., Dordrecht.
2. Boekema, E. J., Dekker, J. P., van Heel, M. G., Rögner, M., Saenger, W., Witt, I., and Witt, H. T. (1987) *FEBS Lett. 217*, 283−286.
3. Ford, R. C., and Holzenburg, A. (1988) *EMBO J. 7*, 2287−2293.
4. Brettel, K. (1997) *Biochim. Biophys. Acta 1318*, 322−373.
5. Schubert, W.-D., Klukas, O., Krauss, N., Saenger, W., Fromme, P., and Witt, H.-T. (1997) *J. Mol. Biol. 272*, 741−769.
6. Falzone, C. J., Kao, Y.-H., Zhao, J., Bryant, D. A., and Lecomte, J. T. J. (1994) *Biochemistry 33*, 6052−6062.
7. Lagoutte, B., and Vallon, O. (1992) *Eur. J. Biochem. 205*, 1175−1185.
8. Zilber, A. L., and Malkin, R. (1992) *Plant Physiol. 99*, 901−911.
9. Kruip, J., Chitnis, P. R., Lagoutte, B., Rögner, M., and Boekema, E. J. (1997) *J. Biol. Chem. 272*, 17061−17069.
10. Zanetti, G., and Merati, G. (1987) *Eur. J. Biochem. 169*, 143−146.
11. Zilber, A. L., and Malkin, R. (1988) *Plant Physiol. 88*, 810−814.
12. Lelong, C., Sétif, P., Lagoutte, B., and Bottin, H. (1994) *J. Biol. Chem. 269*, 10034−10039.
13. Lelong, C., Boekema, E. J., Kruip, J., Bottin, H., Rögner, M., and Sétif, P. (1996) *EMBO J. 15*, 2160−2168.
14. Andersen, B., Koch, B., and Scheller, H. V. (1992) *Physiol. Plant 84*, 154−161.
15. Sonoike, K., Hatanaka, H., and Satoh, S. (1993) *Biochim. Biophys. Acta 1141*, 52−57.
16. Rousseau, F., Sétif, P., and Lagoutte, B. (1993) *EMBO J. 12*, 1755−1765.
17. Chitnis, P. R., Reilly, P. A., Miedel, M. C., and Nelson, N. (1989) *J. Biol. Chem. 264*, 18374−18380.
18. Zhao, J., Snyder, W. B., Mühlenhoff, U., Rhiel, E., Warren, P. V., Golbeck, J. H., and Bryant, D. A. (1993) *Mol. Microbiol. 9*, 183−194.
19. Yu, L., Zhao, J. D., Muhlenhoff, U., Bryant, D. A., and Golbeck, J. H. (1993) *Plant Physiol. 103*, 171−180.
20. Chitnis, P. R., Reilly, P. A., and Nelson, N. (1989) *J. Biol. Chem. 264*, 18381−18385.
21. Xu, Q., Jung, Y.-S., Chitnis, V. P., Guikema, J. A., Golbeck, J. H., and Chitnis, P. R. (1994) *J. Biol. Chem. 269*, 21512−21518.
22. Chitnis, V. P., Jung, Y.-S., Albee, L., Golbeck, J. H., and Chitnis, P. R. (1996) *J. Biol. Chem. 271*, 11772−11780.
23. Hanley, J., Sétif, P., Bottin, H., and Lagoutte, B. (1996) *Biochemistry 35*, 8563−8571.
24. Sétif, P., and Bottin, H. (1994) *Biochemistry 33*, 8495−8504.
25. Sétif, P., and Bottin, H. (1995) *Biochemistry 34*, 9059−9070.
26. Kruip, J., Boekema, E. J., Bald, D., Boonstra, A. F., and Rögner, M. (1993) *J. Biol. Chem. 268*, 23353−23360.
27. Bottin, H., and Lagoutte, B. (1992) *Biochim. Biophys. Acta 1101*, 48−56.
28. Lelong, C., Sétif, P., Bottin, H., André, F., and Neumann, J.-M. (1995) *Biochemistry 34*, 14462−14473.
29. Golbeck, J. H., and Cornelius, J. M. (1986) *Biochim. Biophys. Acta 849*, 16−24.
30. Warren, P. V., Golbeck, J. H., and Warden, J. T. (1993) *Biochemistry 32*, 849−857.
31. Brettel, K., and Golbeck, J. H. (1995) *Photosynth. Res. 45*, 183−193.
32. Mathis, P., and Sétif, P. (1981) *Isr. J. Chem. 21*, 316−320.
33. Margoliash, E., and Bosshard, H. R. (1983) *Trends Biochem. Sci. 8*, 316−320.
34. Schreiber, G., and Fersht, A. R. (1996) *Nature Struct. Biol. 3*, 427−431.
35. Janin, J. (1997) *Proteins 28*, 153−161.
36. Marcus, R. A., and Sutin, N. (1985) *Biochim. Biophys. Acta 811*, 265−322.
37. Moser, C. C., Keske, J. M., Warncke, K., Farid, R. S., and Dutton, P. L. (1992) *Nature 355*, 796−802.
38. Xu, Q., Guikema, J. A., and Chitnis, P. R. (1994) *Plant Physiol. 106*, 617−624.
39. Li, N., Zhao, J., Warren, P. V., Warden, J. T., Bryant, D. A., and Golbeck, J. H. (1991) *Biochemistry 30*, 7863−7872.
40. Fischer, N., Hippler, M., Sétif, P., Jacquot, J.-P., Rochaix, J.-D. (1998) *EMBO J. 17*, 849−858.
41. Andersen, B., Scheller, H. V., and Moller, B. L. (1992) *FEBS Lett. 311*, 169−173.
42. Schluchter, W. M., and Bryant, D. A. (1992) *Biochemistry 31*, 3092−3102.
43. Bald, D., Kruip, J., and Rögner, M. (1996) *Photosynth. Res. 49*, 103−118.

BI981379T